J|A|C|S ARTICLES

Published on Web 12/11/2008

Control of Charge Transfer Phase Transition and Ferromagnetism by Photoisomerization of Spiropyran for an Organic−Inorganic Hybrid System, (SP)[$Fe^{II}Fe^{III}(dto)_3$] (SP = spiropyran, dto = $C_2O_2S_2$)

Noriyuki Kida,*,† Masanori Hikita,† Izuru Kashima,† Masashi Okubo,‡ Miho Itoi,§ Masaya Enomoto,† Kenichi Kato,⊥ Masaki Takata,⊥ and Norimichi Kojima*,†

Graduate School of Arts and Sciences, The University of Tokyo, Komaba 3-8-1, Meguro, Tokyo 153-8902, Japan, Department of Applied Chemistry, The Chuo University, Kasuga 1-13-27, Bunkyo, Tokyo 112-8551, Japan, Department of Physics and Mathematics, Aoyama University, Fuchinobe 5-10-1, Sagamihara, Kanagawa 229-8558, Japan, and RIKEN SPring-8 Center, Koto 1-1-1, Sayo-Cho, Sayo-gun, Hyogo 679-5148, Japan

Received August 30, 2008; E-mail: cnori@mail.ecc.u-tokyo.ac.jp; cc67904@mail.ecc.u-tokyo.ac.jp

Abstract: Iron mixed-valence complex, $(n\text{-}C_3H_7)_4N[Fe^{II}Fe^{III}(dto)_3]$(dto = $C_2O_2S_2$), shows a spin entropy-driven phase transition called charge transfer phase transition in $[Fe^{II}Fe^{III}(dto)_3]^-_\infty$ around 120 K and a ferromagnetic transition at 7 K. These phase transitions remarkably depend on the hexagonal ring size in the two-dimensional honeycomb network structure of $[Fe^{II}Fe^{III}(dto)_3]^-_\infty$. In order to control the magnetic properties and the electronic state in the dto-bridged iron mixed-valence system by means of photoirradiation, we have synthesized a photosensitive organic−inorganic hybrid system, (SP)$[Fe^{II}Fe^{III}(dto)_3]$(SP = spiropyran), and investigated the photoinduced effect on the magnetic properties. Upon UV irradiation at 350 nm, a broad absorption band between 500 and 600 nm appears and continuously increases with the photoirradiation time, which implies that the UV irradiation changes the structure of spiropyran from the closed form to the open one in solid state. The photochromism in spiropyran changes the ferromagnetic transition temperature from 5 to 22 K and the coercive force from 1400 to 6000 Oe at 2 K. In this process, the concerted phenomenon coupled with the charge transfer phase transition in $[Fe^{II}Fe^{III}(dto)_3]^-_\infty$ and the photoisomerization of spiropyran is realized.

1. Introduction

Current research in the field of molecular solids is investigating the possibilities of an organic−inorganic hybrid system having multifunctionality coupling with transport, optical, or magnetic properties. Multifunctional materials are expected to provide a unique interplay between these physical properties, such as phototunable conductivity[1] or field-induced superconductivity.[2] Among these multifunctional materials based on molecular solids, both from the fundamental and applied points of view, extensive studies have been performed for various photoinduced phenomena such as the light-induced excited spin-state trapping (LIESST) in spin-crossover complexes,[3,4] the photoinduced magnetism in transition metal cyanides,[5] the photoinduced valence tautomerism in Co complexes,[6] the photoinduced valence transition for halogen-bridged gold mixed-valence complexes[7] and iodine-bridged binuclear Pt complexes,[8] the photoinduced transition between the metallic and insulating

† The University of Tokyo.
‡ The Chuo University.
§ Aoyama University.
⊥ RIKEN SPring-8 Center.

(1) Tajima, N.; Fujisawa, J.; Naka, N.; Ishihara, T.; Kato, R.; Nishio, Y.; Kajita, K. *J. Phys. Soc. Jpn.* **2005**, *74*, 511.
(2) (a) Uji, S.; Shinagawa, H.; Terashima, T.; Yakabe, T.; Terai, Y.; Tokumoto, M.; Kobayashi, A.; Tanaka, H.; Kobayashi, H. *Nature* **2001**, *410*, 908. (b) Uji, S.; Terashima, T.; Terakura, C.; Yakabe, T.; Terai, Y.; Yasuzuka, S.; Imanaka, Y.; Tokumoto, M.; Kobayashi, A.; Sakai, F.; Tanaka, H.; Kobayashi, H.; Balicas, L.; Brooks, J. S. *J. Phys. Soc. Jpn.* **2003**, *72*, 369.
(3) (a) Decurtins, S.; Gütlich, P.; Köhler, C. P.; Spiering, H.; Hauser, A. *Chem. Phys. Lett.* **1984**, *105*, 1. (b) Decurtins, S.; Gütlich, P.; Hasselbach, K. M.; Hauser, A.; Spiering, H. *Inorg. Chem.* **1985**, *24*, 2174.
(4) Gütlich, P.; Goodwin, H. A. *Spin Crossover in Transition Metal Compounds I−III*, Springer: New York, 2004. and related refs therein.
(5) (a) Sato, O.; Iyoda, T.; Fujishima, A.; Hashimito, K. *Science* **1996**, *272*, 704. (b) Einaga, Y.; Sato, O.; Iyoda, T.; Kobashi, Y.; Ambe, F.; Hashimoto, K.; Fujishima, A. *Chem. Lett.* **1997**, 289. (c) Bleuzen, A.; Lomenech, C.; Escax, V.; Villain, F.; Varret, F.; Moulin, C.; Verdaguer, M. *J. Am. Chem. Soc.* **2000**, *122*, 6648. (d) Varret, F.; Bleuzen, A.; Boukheddaden, K.; Bousseksou, A.; Codjovi, E.; Enachescu, C.; Goujon, A.; Linares, J.; Menendez, N.; Verdaguer, M. *Pure Appl. Chem.* **2002**, *74*, 2159. (e) Li, G.; Akitsu, T.; Sato, O.; Einaga, Y. *J. Am. Chem. Soc.* **2003**, *125* (41), 12396. (f) Dei, A. *Angew. Chem., Int. Ed.* **2005**, *44*, 1160.
(6) (a) Carbonera, C.; Dei, A.; Létard, J. F.; Sangregorio, C.; Sorace, L. *Angew. Chem., Int. Ed.* **2004**, *43*, 3135. (b) Dei, A.; Gatteschi, D.; Sangregorio, C.; Sorace, L. *Acc. Chem. Res.* **2004**, *37* (11), 827. (c) Sato, O.; Cui, A.; Matsuda, R.; Tao, J.; Hayami, S. *Acc. Chem. Res.* **2007**, *40* (5), 361. (d) Sato, O.; Tao, J.; Zhang, Y. J. *Angew. Chem., Int. Ed.* **2007**, *46*, 2152.
(7) (a) Liu, X. J.; Moritomo, Y.; Nakamura, A.; Kojima, N. *J. Phys. Soc. Jpn.* **1999**, *68*, 3134. (b) Son, J.-Y.; Mizokawa, T.; Quilty, J. W.; Takubo, K.; Ikeda, K.; Kojima, N. *Phys. Rev. B: Condens. Mater. Chem.* **2005**, *72*, 235105.
(8) Matsuzaki, H.; Matsuoka, T.; Kishida, H.; Takizawa, K.; Miyasaka, H.; Sugiura, K.; Yamashita, M.; Okamoto, H. *Phys. Rev. Lett.* **2003**, *90*, 046401.

 10.1021/ja806879a CCC: $40.75

phases for organic salts,[9] and so forth. Among various multifunctional materials, a molecular-based magnet is a leading candidate as a photocontrollable multifunctional material. Intercalated magnetic compounds such as layered double hydroxides (LDHs),[10−12] oxalato-bridged bimetal complexes $A[M^{II}M'^{III}(ox)_3]$ (A = cation, M, M′ = metal, ox = C_2O_4),[13−17] dithiooxalato-bridged bimetal complexes $A[M^{II}M'^{III}(dto)_3]$ (A = cation, M, M′ = metal, dto = $C_2S_2O_2$),[18−27] perovskite-type metal halides $A_2M^{II}X_4$ (A = cation, M = metal, X = halogen),[28−30] magnetic vesicles,[31−33] or magnetic thin films[34−36] provide an excellent opportunity to control their magnetic properties by the intercalation of various molecules.

In the case of dithiooxalato-bridged bimetal complexes $A[M^{II}M'^{III}(dto)_3]$, recently we have discovered a new type of phase transition around 120 K for $(n\text{-}C_3H_7)_4N[Fe^{II}Fe^{III}(dto)_3]$ (dto = $C_2O_2S_2$), where the thermally induced charge transfer between Fe^{II} and Fe^{III} occurs reversibly in order to minimize the free energy in the whole system.[18−20] $(n\text{-}C_3H_7)_4N[Fe^{II}Fe^{III}(dto)_3]$ has a two-dimensional honeycomb network structure with an alternating array of Fe^{II} and Fe^{III} atoms through dto bridges, and the $(n\text{-}C_3H_7)_4N^+$ cation layers are intercalated between two $[Fe^{II}Fe^{III}(dto)_3]^-_\infty$ layers.[23,24] In the higher-temperature phase (T > 120 K), the Fe^{III}(S = $^1/_2$) and Fe^{II}(S = 2) sites are coordinated by six S atoms and six O atoms, respectively. In the lower-temperature phase (T < 120 K), on the other hand, the Fe^{III}(S = $^5/_2$) and Fe^{II}(S = 0) sites are coordinated by six O atoms and six S atoms, respectively. $(n\text{-}C_4H_9)_4N[Fe^{II}Fe^{III}(dto)_3]$ also undergoes the charge transfer phase transition between 200 and 80 K (transition temperature of the charge transfer phase transition T_{CT} = 140 K), while the charge transfer phase transition does not take place for $(n\text{-}C_nH_{2n+1})_4N[Fe^{II}Fe^{III}(dto)_3]$ (n = 5 and 6), where the spin configuration of Fe^{II} (S = 2) and Fe^{III} (S = $^1/_2$) is stable between 2 and 300 K.[25] Moreover, $(n\text{-}C_nH_{2n+1})_4N[Fe^{II}Fe^{III}(dto)_3]$ (n = 3−6) undergo the ferromagnetic phase transition. The Curie temperatures T_C for n = 3 and 4 are 7 and 7 K (and 13 K), respectively, while those for n = 5 and 6 are 19.5 and 22 K, respectively.[25] The Curie temperatures for n = 3 and 4 are quite lower than those for n = 5 and 6, which is attributed to that the Fe^{II} site in the lower temperature phase for n = 3 and 4 is diamagnetic low spin state. In the case of n = 4, two ferromagnetic phases with T_C = 7 K and T_C = 13 K corresponding to the ferromagnetic phases in the lower- and higher-temperature phases coexist.

As mentioned above, the charge transfer phase transition and the ferromagnetic transition in $(n\text{-}C_nH_{2n+1})_4N[Fe^{II}Fe^{III}(dto)_3]$ remarkably depend on the size of intercalated cation, which implies a possibility to control the magnetic properties of two-dimensional honeycomb network structure of $[Fe^{II}Fe^{III}(dto)_3]^-_\infty$ by means of the isomerization of intercalated cation. In organic−inorganic hybrid systems, it is effective to use an organic photochromic molecule for producing photoswitchable materials. On the basis of this strategy, we have used a photochromic spiropyran (SP) as the intercalated cation for dithiooxalato-bridged iron mixed-valence complex, $[Fe^{II}Fe^{II}_{1-\iota}(dto)_3]$, and have tried to control the charge transfer phase transition and the ferromagnetism for $(SP)[Fe^{II}Fe^{III}(dto)_3]$ by means of photoisomerization of SP.

In connection with this, the following should be mentioned. Although photochromic properties of SP have been largely investigated, photochromic SP in the solid state is very rare. Recently, two cationic pyrido-spiropyrans were found to show the photochromism in the crystalline state.[37] Soon after that, organic−inorganic hybrid complexes, $(SP)[MnCr(ox)_3]\cdot H_2O$[38] and $(SP)[Fe^{II}Fe^{III}(dto)_3]$[39] were synthesized and found to show the photoisomerization of SP^+ in the crystalline state. In both

(9) (a) Uchida, N.; Koshihara, S.; Ishikawa, T.; Ota, A.; Fukaya, S.; Matthieu, C.; Yamochi, H.; Saito, G. *J. Phys. IV France* **2004**, *114*, 143. (b) Chollet, M.; Guerin, L.; Uchida, N.; Fukaya, S.; Shimoda, H.; Ishikawa, T.; Matsuda, K.; Hasegawa, T.; Ohta, A.; Yamochi, H.; Saito, G.; Tazaki, R.; Adachi, S.; Koshihara, S. *Science* **2005**, *307*, 86.

(10) (a) Laget, V.; Hornick, C.; Rabu, P.; Drillon, M.; Ziessel, R. *Coord. Chem. Rev.* **1998**, *178*, 1533. (b) Rabu, P.; Huang, Z. L.; Hornick, C.; Drillon, M. *Synth. Met.* **2001**, *122*, 509.

(11) (a) Okubo, M.; Enomoto, M.; Kojima, N. *Solid State Commun.* **2005**, *134*, 777. (b) Shimizu, H.; Okubo, M.; Nakamoto, A.; Enomoto, M.; Kojima, N. *Inorg. Chem.* **2006**, *45*, 10240.

(12) Fujita, W.; Awaga, K. *J. Am. Chem. Soc.* **1997**, *119*, 4563.

(13) (a) Tamaki, H.; Zhong, Z. J.; Matsumoto, N.; Kida, S.; Koikawa, M.; Achiwa, N.; Hashimoto, Y.; Ōkawa, H. *J. Am. Chem. Soc.* **1992**, *114*, 6974. (b) Tamaki, H.; Mitsumi, M.; Nakamura, K.; Matsumoto, N.; Kida, S.; Ōkawa, H.; Iijima, S. *Chem. Lett.* **1992**, 1975.

(14) (a) Decurtins, S.; Schmalle, H. W.; Oswald, H. R.; Linden, A.; Ensling, J.; Gütlich, P.; Hauser, A. *Inorg. Chim. Acta* **1994**, *216*, 65. (b) Clement, R.; Decurtins, S.; Gruselle, M.; Train, C. *Monatsh. Chem.* **2003**, *134*, 117.

(15) Mathonière, C.; Nuttall, C. J.; Carling, S. G.; Day, P. *Inorg. Chem.* **1996**, *35*, 1201.

(16) Coronado, E.; Galán-Mascarós, J. R.; Gómez-García, C. J.; Ensling, J.; Gütlich, P. *Chem. Eur. J.* **2000**, *6*, 552.

(17) Coronado, E.; Galán-Mascarós, J. R.; Gómez-García, C. J.; Laukhin, V. *Nature* **2000**, *408*, 447.

(18) Ōkawa, H.; Mitsumi, M.; Ohba, M.; Kodera, M.; Matsumoto, N. *Bull. Chem. Soc. Jpn.* **1994**, *67*, 2139.

(19) Kojima, N.; Aoki, W.; Itoi, M.; Seto, M.; Kobayashi, Y.; Maeda, Yu *Solid State Commun.* **2001**, *120*, 165.

(20) Nakamoto, T.; Miyazaki, Y.; Itoi, M.; Ono, Y.; Kojima, N.; Sorai, M. *Angew. Chem., Int. Ed.* **2001**, *40*, 4716.

(21) Kojima, N.; Aoki, W.; Seto, M.; Kobayashi, Y.; Maeda, Yu *Synth. Met.* **2001**, *121*, 1796.

(22) Kojima, N.; Itoi, M.; Ono, Y.; Okubo, M.; Enomoto, M. *Mater. Sci.* **2003**, *21*, 181.

(23) Bradley, J. M.; Carling, S. G.; Visser, D.; Day, P.; Hautot, D.; Long, G. J. *Inorg. Chem.* **2003**, *42*, 986.

(24) Ono, Y.; Okubo, M.; Kojima, N. *Solid State Commun.* **2003**, *126*, 291.

(25) Itoi, M.; Taira, A.; Enomoto, M.; Matsushita, N.; Kojima, N.; Kobayashi, Y.; Asai, K.; Koyama, K.; Nakamoto, T.; Uwatoko, Y.; Yamamura, J. *Solid State Commun.* **2004**, *130*, 415.

(26) (a) Itoi, M.; Doctoral Thesis, The University of Tokyo, Japan, 2004. (b) Itoi, M.;Ono, Y.;Kojima, N.;Kato, K.;Osaka, K.;Takata, M.;*Eur. J. Inorg. Chem.* **2006,** *2006,* 1198.

(27) Kojima, N.; Ono, Y.; Kobayashi, K.; Seto, M. *Hyperfine Interact.* **2004**, *156−157*, 175.

(28) de Jongh, L. J.; Van Amstel, W. D.; Miedema, A. R. *Physica* **1972**, *58*, 277.

(29) Landee, C. P.; Halvorson, K. E.; Willett, R. D. *J. Appl. Phys.* **1987**, *61*, 3295.

(30) de Jongh, L. J., Ed. *Magnetic Properties of Layered Transition Metal Compounds*; Kluwer Academic Publishers: Dordrecht, 1990.

(31) Einaga, Y.; Sato, O.; Iyoda, T.; Fujishima, A.; Hashimoto, K. *J. Am. Chem. Soc.* **1999**, *121*, 3745.

(32) (a) Einaga, Y; Taguchi, M.; Li, G.; Akitsu, T.; Gu, Z.-Z.; Sugai, T.; Sato, O. *Chem. Mater.* **2003**, *15*, 8. (b) Taguchi, M.; Li, G.; Gu, Z.; Sato, O.; Einaga, Y. *Chem. Mater.* **2003**, *15*, 4756.

(33) Mikami, R.; Taguchi, M.; Yamada, K.; Suzuki, K.; Sato, O.; Einaga, Y. *Angew. Chem., Int. Ed.* **2004**, *43*, 6135.

(34) Yamamoto, T.; Umemura, Y.; Sato, O.; Einaga, Y. *Chem. Mater.* **2004**, *16*, 1195.

(35) Yamamoto, T.; Umemura, Y.; Sato, O.; Einaga, Y. *J. Am. Chem. Soc.* **2005**, *127*, 16065.

(36) Suda, M.; Miyazaki, Y.; Hagiwara, Y.; Sato, O.; Shiratori, S.; Einaga, Y. *Chem. Lett.* **2005**, *34*, 1028.

(37) Bénard, S.; Yu, P. *Adv. Mater.* **2000**, *12*, 48.

(38) Bénard, S.; Rivière, E.; Yu, P.; Nakatani, K.; Delouis, J. F. *Chem. Mater.* **2001**, *13*, 159.

(39) Kashima, I.; Okubo, M.; Ono, Y.; Itoi, M.; Kida, N.; Hikita, M.; Kojima, N. *Synth. Met.* **2005**, *153*, 473.

Scheme 1. Photochromism of Cationic Spiropyran (SP-R)

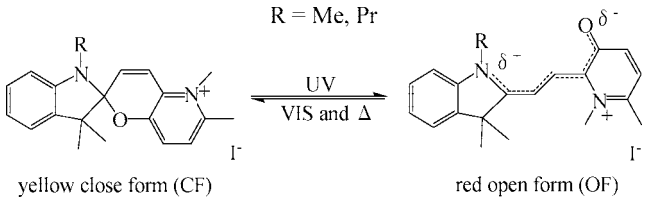

Scheme 2. Schematic Representation of $[Fe^{II}Fe^{III}(dto)_3]^-_\infty$

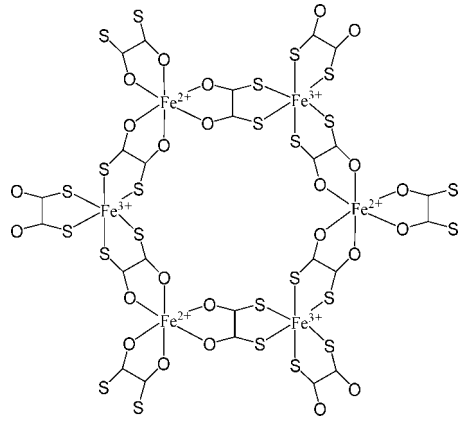

cases, the coercive force is enhanced by UV irradiation, but any modulation of the Curie temperature has not been reported.

In this paper, we report the synthesis of photosensitive organic−inorganic hybrid complexes, (SP-R)$[Fe^{II}Fe^{III}(dto)_3]$ (SP-R = cationic spiropyran shown in Scheme 1, R = methyl (Me), propyl (Pr)), the photoisomerization of $SP\text{-}R^+$ in the solid state and the photoinduced effect on the charge transfer phase transition and the ferromagnetic transition by the measurements of magnetic susceptibility and UV−vis spectroscopy. (SP-R)$[Fe^{II}Fe^{III}(dto)_3]$ consists of a cationic spiropyran ($SP\text{-}R^+$: Scheme 1) and the two-dimensional honeycomb network structure of $[Fe^{II}Fe^{III}(dto)_3]^-_\infty$ (Scheme 2). In general, the cationic spiropyran is converted from the yellow-colored closed form (CF) to the red-colored open form (OF) upon the irradiation of UV light (330−370 nm) at room temperature. The OF is usually less stable and returns to the closed form both thermally and photochemically (500−600 nm) in solution. However, as mentioned later, the open form of $SP\text{-}R^+$ is stable in (SP-R)$[Fe^{II}Fe^{III}(dto)_3]$.

2. Experimental Section

Synthesis. Reagents were of commercial grade. (SP-R)I (R = Me, Pr) was synthesized according to the literature.[37,40]

Preparation of Neutral Pyrido-Spiropyran SP-Me. In 40 mL of ethanol were refluxed for 3 h the following: 1.37 g (10 mmol) of 3-hydroxy-6-methyl-2-pyridinecarboxaldehyde and 1.73 g (10 mmol) of 2-methylene-1,3,3-trimethylindoline. The ethanol was evaporated, and then ∼30 mL of water was added to the reaction mixture. The mixture was stirred for several hours, and the pale colored precipitate was filtered, washed with water, and dried (70% yield).

Preparation of (SP-Me)I. In 40 mL of THF were refluxed overnight the following: 1.46 g (5 mmol) of SP-Me and 3.1 mL (50 mmol) of methyl iodide. The solution was allowed to cool down to room temperature, and the yellow microcrystalline solid was filtered, washed with THF, and dried (64% yield). Elemental Analysis calculated for $C_{20}H_{23}N_2OI$: C, 55.31; H, 5.34; N, 6.45. Found: C, 55.48; H, 5.61; N, 6.23.

Preparation of (SP-Pr)I. Four grams (25 mmol) of 2,3,3-trimethylindolenine and 2.4 mL (25 mmol) of propyl iodide were refluxed for 7 h in 70 mL of acetonitrile to give 1-propyl-2,3,3-trimethylindolenium iodide as red colored powder (65% yield). To the solution of 25 mL of water and 9 mL of chloroform was added dropwise 50% aqueous NaOH solution, and the reaction mixture was stirred for 2 h at room temperature, which was then extracted using chloroform. The solution was dried with anhydrous magnesium sulfate and concentrated under reduced pressure to give 1-propyl-3,3-methyleneindoline as red colored liquid (41% yield). Then (SP-Pr)I was prepared by using the same procedure described for (SP-Me)I as yellow powdered crystals (26% yield). Elemental Analysis calculated for $C_{22}H_{27}N_2OI$: C, 57.15; H, 5.89; N, 6.06. Found: C, 57.43; H, 6.07; N, 5.97.

Preparation of (SP-Me)$[Fe^{II}Fe^{III}(dto)_3]$ (1) and (SP-Pr)-$[Fe^{II}Fe^{III}(dto)_3]$ (2). $KBa[Fe(dto)_3]\cdot 3H_2O$ was prepared in a way similar to that reported in the literature.[26] A solution (20 mL) of $FeCl_2\cdot 4H_2O$ (0.15 g, 0.78 mmol) and (SP-Me)I (0.50 g, 1.17 mmol) in a methanol−water mixture of 3: 2 ratio was stirred. To this, a solution (30 mL) of $KBa[Fe(dto)_3]\cdot 3H_2O$ (0.50 g, 0.78 mmol) in a methanol−water mixture of 3: 2 ratio was added. In this way, **1** was obtained as black colored precipitate. The compound was separated as powdered crystals by suction filtration and washed first with a 1:1 methanol/water mixture and then with methanol and diethyl ether. Yield: ∼30%. Elemental Analysis calculated for $C_{26}H_{23}N_2O_7S_6Fe_2$: C, 40.06; H, 2.97; N, 3.59; S, 24.68. Found: C, 39.77; H, 3.03; N, 3.32; S, 24.61. **2** was synthesized in the similar way. Yield: ∼30%. Elemental Analysis calculated for $C_{28}H_{27}N_2O_7S_6Fe_2$: C, 41.64; H, 3.37; N, 3.47; S, 23.83. Found: C, 41.34; H, 3.33; N, 3.11; S, 23.48.

Preparation of (SP-Me)$[Co^{II}Fe^{III}(dto)_3]$ (3) and (SP-Pr)-$[Co^{II}Fe^{III}(dto)_3]$ (4). 3 and **4** were synthesized in a way similar to that for the preparation of **1** and **2** using $CoCl_2\cdot 6H_2O$ as the Co^{II} source. Yield: ∼30%. Elemental Analysis calculated for $C_{26}H_{23}N_2O_7S_6FeCo$: C, 39.90; H, 2.96; N, 3.58; S, 24.59. Found: C, 39.61; H, 3.11; N, 3.37; S, 24.55 and $C_{28}H_{27}N_2O_7S_6FeCo$: C, 41.48; H, 3.36; N, 3.46; S, 23.73. Found: C, 41.41; H, 3.43; N, 3.19; S, 23.85.

The IR spectra were measured with a JASCO IR Report-100 at room temperature. The powder X-ray diffraction profiles for **1**, **3**, and **4** were measured with Rigaku multiflex at room temperature. The powder X-ray diffraction data of **2** were taken at the BL02B2 beam line of SPring-8.[41] The powdered sample was sealed in a Lindemann capillary having a diameter of 0.3 mm, which gave a homogeneous intensity distribution in the Debye−Scherrer ring. The wavelength of the X-ray was 1.001 Å, and the exposure time at 300 K was 1 h. The UV−vis spectra were monitored with a JASCO MSV-370 by KBr method at room temperature and 70 K. Temperature was controlled by an Oxford CRYOMINI and an Oxford ITC503S temperature controller. For ^{57}Fe Mössbauer spectroscopic measurement, ^{57}Co in Rh was used as a Mössbauer source. The spectra were calibrated by using the six lines of a body-centered cubic iron foil (α-Fe), the center of which was taken as zero isomer shift. The static magnetic susceptibility was measured by a Quantum Design MPMS5 SQUID susceptometer under 5000 Oe. The zero field cooled magnetization (ZFCM) and field cooled magnetization (FCM) were also measured for the investigation of the ferromagnetic phase in the temperature range of 2−30 K under 30 Oe. The remnant magnetization (RM) was measured in the same temperature region under zero field. Field dependence of the magnetization was measured at 2 K in the field range of −50000 Oe ≤ H ≤ 50000 Oe. The powder sample of 10 mg was wrapped

(40) Kim, S. H.; Suh, H. J.; Cui, J. Z.; Gal, Y. S.; Jin, S. H.; Koh, K. *Dyes Pigments* **2002**, *53*, 251.

(41) Nishibori, E.; Takata, M.; Kato, K.; Sakata, M.; Kubota, Y.; Aoyagi, S.; Kuroiwa, Y.; Yamamoto, M.; Ikeda, N. *Nucl. Instrum. Methods Phys. Res. A* **2001**, *1045−1048*, 467.

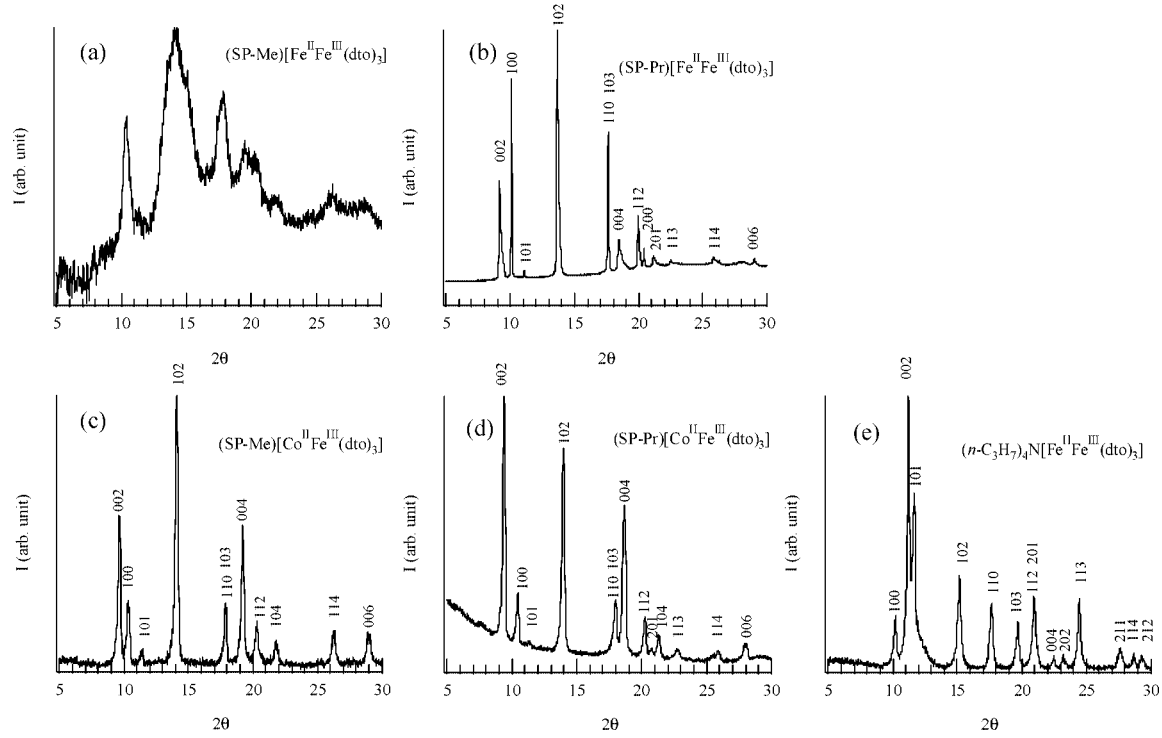

Figure 1. X-ray powder diffraction profiles of (a) **1**, (b) **2**, (c) **3**, (d) **4**, and (e) $(n\text{-}C_3H_7)_4N[Fe^{II}Fe^{III}(dto)_3]$ for reference. The 2θ values of (b) are transformed into those derived from λ(Cu Kα_1).

in polyethylene film and held in a plastic straw. The magnetic susceptibility obtained was corrected for the background and the core diamagnetism estimated from Pascal's constants. The sample irradiation was performed with a Xe lamp [Asahi Spectra Co. LAX-101 (350 nm, 40 mW/cm^2)] as the UV source using band-pass filters and a halogen lamp (Hoya-Schott MEGALIGHT 100-S) as the visible light source (600 mW/cm^2).

3. Results and Discussion

All the compounds prepared were characterized by infrared spectra and X-ray powder diffraction at room temperature. In the infrared spectra of the compounds, the characteristic antisymmetric C−O stretching mode appears as single intense bands at 1489, 1490, 1492, and 1492 cm^{-1} for **1**−**4**, respectively. These values are relatively lower than for the parent compounds K_2(dto) and KBa[Fe(dto)$_3$]$\cdot 3H_2O$, whose C−O vibration modes appear at 1516 and 1528 cm^{-1}, respectively. This feature indicates that all of the dithiooxalate groups in **1**−**4** act as bridging ligands,[42] which is consistent with the above-described structure of the dithiooxalate layers. The X-ray powder diffraction profiles are shown in Figure 1. Each profile shows a similar pattern, while **1** exhibits broad peaks, indicating a quite disordered structure. The reflections for **2**, **3**, and **4** are indexed using a hexagonal unit cell just like most dto-bridged bimetal compounds with 2-D honeycomb network structure, $A[M^{II}M'^{III}(dto)_3]$ ($A = (n\text{-}C_nH_{2n+1})_4N$, $(n\text{-}C_nH_{2n+1})_4P$, M = Mn, Co, Ni, Fe, M′ = Cr, Fe), previously studied.[23−26] The unit cell parameters are given in Table 1. Although it is difficult to decide the precise crystal structure of **1**, it might be isostructural with **2**−**4** since the peaks over the range 10°−22° suggest a hexagonal unit cell. The ^{57}Fe Mössbauer spectra of **1** and $(n\text{-}C_3H_7)_4N[Fe^{II}Fe^{III}(dto)_3]$ at room temperature are shown in Figure 2. The line profiles of the complexes are quite similar to each other and two quadrupole doublets are assigned to Fe^{II} ($S = 2$) and Fe^{III} ($S = {}^1/_2$). The Mössbauer parameters are summarized in Table 2. The values of the isomer shifts and quadrupole splittings of **1** are very close to those of $(n\text{-}C_nH_{2n+1})_4N[Fe^{II}Fe^{III}(dto)_3]$ compounds with the spin states of Fe^{II} ($S = 2$) and Fe^{III} ($S = {}^1/_2$).[29] According to the infrared and Mössbauer spectra, the 2-D honeycomb network structure of $[Fe^{II}Fe^{III}(dto)_3]^-_\infty$ is formed in **1**, where the Fe^{II} ($S = 2$) and Fe^{III} ($S = {}^1/_2$) sites are coordinated by six O atoms and six S atoms, respectively. Therefore, the intense disorder of the crystal structure in **1** originates from the countercation layer. The values of the *a*-axis lattice parameter for **2**−**4** are very close to those of $(n\text{-}C_3H_7)_4N[Fe^{II}Fe^{III}(dto)_3]$ and $(n\text{-}C_3H_7)_4N[Co^{II}Fe^{III}(dto)_3]$ derived from the single crystal study. This result strongly suggests that the *a*-axis lattice parameter represents the distance of $Fe^{III}-Fe^{III}$ ($Fe^{II}-Fe^{II}$) in the $[Fe^{II}Fe^{III}(dto)_3]^-_\infty$ layer, and the direction of stacking of the layers is along the crystallographic *c*-axis in the compounds **1**−**4** just as for $A[M^{II}M'^{III}(dto)_3]$ already known. The *c*/2 represents the interlayer distance, suggesting the $P6_3$ space group analogous to that for $(n\text{-}C_3H_7)_4N[Fe^{II}Fe^{III}(dto)_3]$ and $(n\text{-}C_3H_7)_4N[Co^{II}Fe^{III}(dto)_3]$.

Table 1. Parameters of the Hexagonal Unit Cell of Selected (SP-R)$[M^{II}Fe^{III}(dto)_3]$ Compounds and $(n\text{-}C_3H_7)_4N[Fe^{II}Fe^{III}(dto)_3]$ [24]

cmpd	*a* (Å)	*c* (Å)
2	10.08(6)	18.63(10)
3	10.01(1)	18.61(1)
4	10.04(2)	19.32(7)
$(n\text{-}C_3H_7)_4N[Fe^{II}Fe^{III}(dto)_3]$	10.0618(5)	16.0424(7)

Figure 3a shows the UV−vis absorption spectra for (SP-Me)I in a KBr pellet. Upon UV irradiation at 350 nm, a broad absorption band between 500 and 650 nm, corresponding to the $\pi-\pi^*$ transition of the OF, appears. This photochromism is based on the UV light-induced equilibrium between the yellow CF and the red OF as shown in Scheme 1.[37] In contrast, the

(42) Coucouvanis, D.; Piltingsrud, D. *J. Am. Chem. Soc.* **1973**, *95*, 5556.

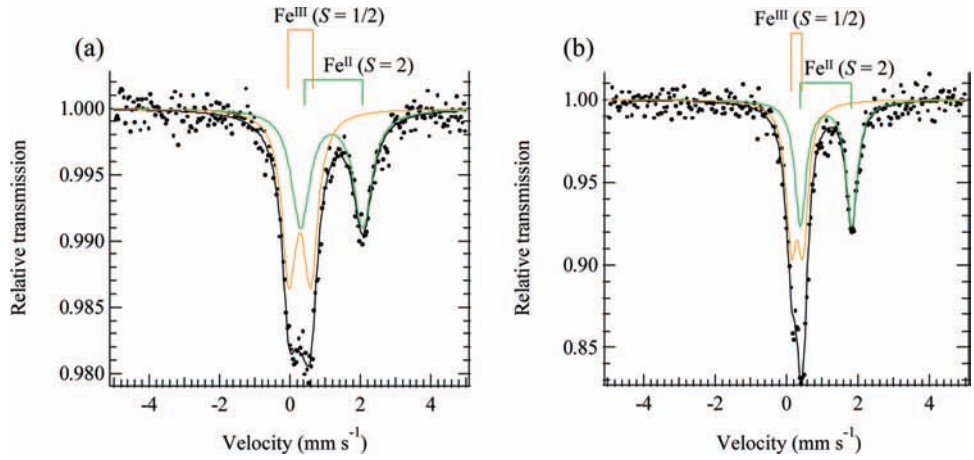

Figure 2. ^{57}Fe Mössbauer spectra of (a) **1** and (b) $(n\text{-}C_3H_7)_4N[Fe^{II}Fe^{III}(dto)_3]$ at room temperature.

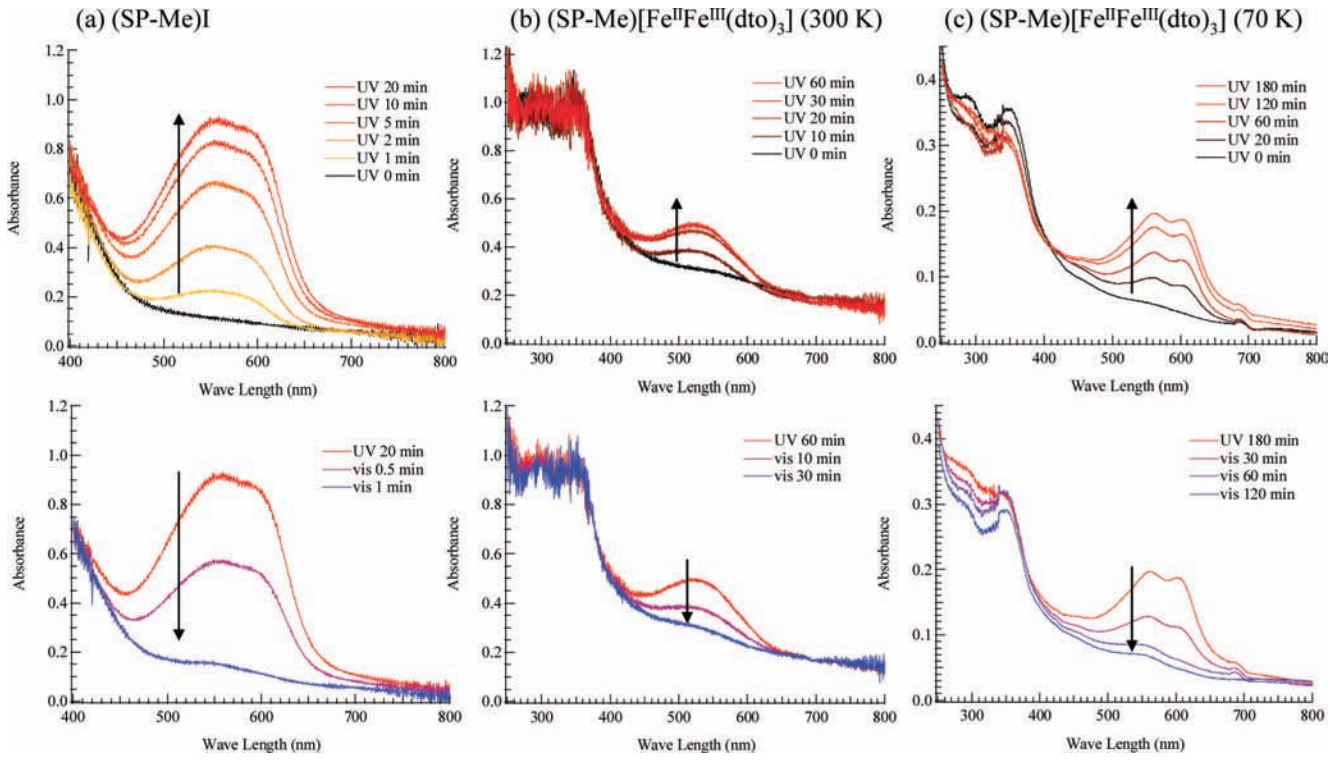

Figure 3. UV−vis spectral change of (a) (SP-Me)I and **1** in KBr pellet at (b) 300 and (c) 70 K. UV irradiation (350 nm, 40 mW/cm^2) on the pellet was carried out first. After the spectra were saturated, visible-light irradiation (600 mW/cm^2) on the pellet was carried out.

Table 2. ^{57}Fe Mössbauer Parameters of **1** and $(n\text{-}C_3H_7)_4N[Fe^{II}Fe^{III}(dto)_3]$

		isomer shift (mm s^{-1})	quadrupole splitting (mm s^{-1})	line width (mm s^{-1})	fraction (%)
1	Fe^{II} ($S = 2$)	1.19	1.77	0.63	48.5
1	Fe^{III} ($S = {}^1/_2$)	0.29	0.61	0.49	51.5
$(n\text{-}C_3H_7)_4N[Fe^{II}Fe^{III}(dto)_3]$	Fe^{II} ($S = 2$)	1.11	1.43	0.38	50.9
$(n\text{-}C_3H_7)_4N[Fe^{II}Fe^{III}(dto)_3]$	Fe^{III} ($S = {}^1/_2$)	0.30	0.33	0.36	49.1

visible-light irradiation returned the saturated spectrum to the original one. Parts b and c of Figure 3 show the changes of the absorption spectra for **1** in KBr pellet upon UV irradiation at 350 nm at 300 and 70 K, respectively. In the case of 300 K, the intensity of the top of the peak around 570 nm is continuously enhanced with the increase of UV irradiation time while the initial black pellet turns deep purple. After the UV irradiation for 30 min, the intensity of the absorption spectrum corresponding to the $\pi-\pi^*$ transition of the OF is almost saturated. The UV light-induced OF of **1** is stable even at room temperature in the dark condition and the purple color slowly fades to return to black in several days. In contrast, visible light irradiation considerably accelerates the color decay. This result implies that the photoisomerization of SP-Me$^+$ from CF to OF by UV irradiation and from OF to CF by visible-light irradiation reversibly takes place in the solid state of **1** at room temperature.

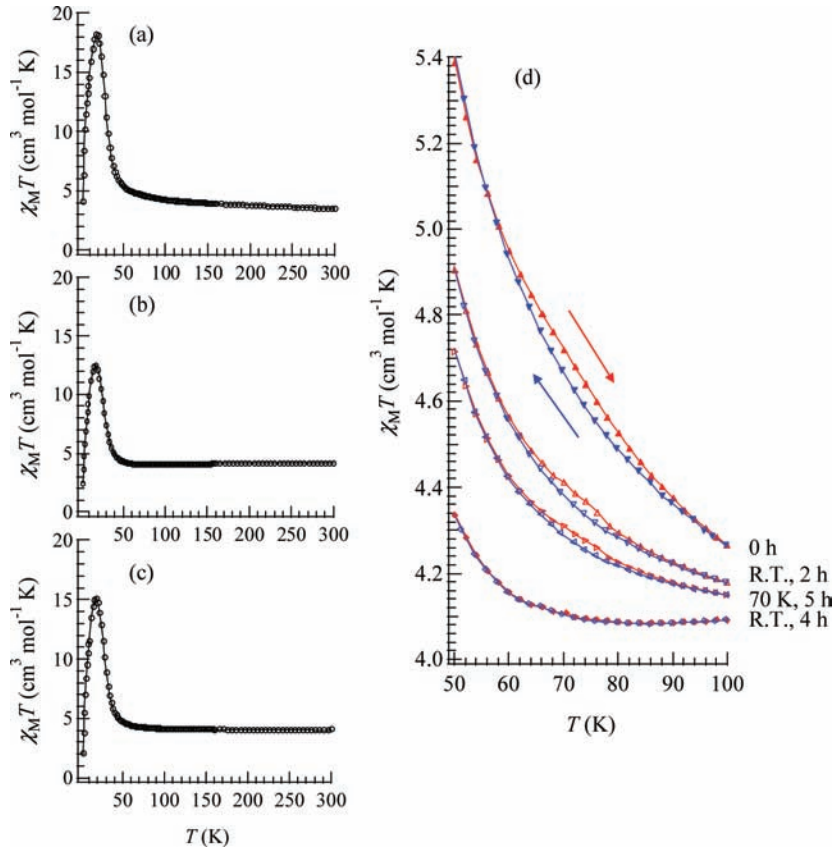

Figure 4. Temperature dependence of $\chi_M T$ of **1** (a) before and after UV irradiation (350 nm, 40 mW/cm^2) at (b) 300 K and (c) 70 K. Applied magnetic field was 5000 Oe. (d) UV irradiation effect on the $\chi_M T$ vs T in the temperature range around the charge transfer phase transition.

At 70 K, the photoisomerization of SP-Me$^+$ is also induced by UV irradiation, and the intensity of the absorption spectrum around 570 nm is almost saturated in 180 min. In this case, the absorption band also almost disappears upon visible-light irradiation for 120 min.

The static magnetic susceptibility of powder samples of **1**−**4** was measured in an external magnetic field of 5000 Oe. Figure 4a shows the product of the molar magnetic susceptibility and temperature, $\chi_M T$, of **1** as a function of temperature. The effective moment at room temperature is 5.28 μ_B which is close to that of the spin only value of the HTP with Fe^{II} ($S = 2$) and Fe^{III} ($S = {}^1/_2$) (5.20 μ_B, $g = 2$). The Curie constant and Weiss constant calculated from the value above 100 K are 3.25 cm^3 mol^{-1} K and +26.2 K, respectively. It is remarkable that the $\chi_M T$ curve exhibits a thermal hysteresis loop between 50 and 100 K showing a small bump around 75 K during the heating process (shown in Figure 4a), which indicates that the charge transfer phase transition occurs as well as in the case of (n-$C_nH_{2n+1})_4N[Fe^{II}Fe^{III}(dto)_3]$ ($n = 3$ and 4) in the similar temperature range. Note that the LTP has a larger magnetization value than the HTP in the vicinity of the charge transfer phase transition in the case of **1**, which is different from (n-$C_nH_{2n+1})_4N[Fe^{II}Fe^{III}(dto)_3]$ ($n = 3$ and 4). This difference presumably arises from the better quenching of the orbital angular momentum in the ground multiplets $^5T_2$ of Fe^{II} and $^2T_2$ of Fe^{III} in **1**. Considering their spin only values (5.92 μ_B for the LTP and 5.20 μ_B for the HTP, g is 2), the LTP has a larger effective moment than the HTP. As the temperature is lowered below 50 K, $\chi_M T$ rapidly increases up to a maximum value around 18 K and the magnetization is saturated below the temperature, which suggests that the compound **1** exhibits a long-range ferromagnetic ordering as well as (n-$C_nH_{2n+1})_4N[Fe^{II}Fe^{III}(dto)_3]$. To confirm and characterize the ferromagnetically ordered phase, we measured the FCM, RM, ZFCM and field dependence of the magnetization. The results are displayed in Figures 5a and 6. The FCM curve decreases stepwise at ∼7 K and disappears at about 25 K. The RM curve also decreases stepwise at 7 K and then disappears at about 22 K. The ZFCM curve, on the other hand, has two maxima at 5 and 18 K. These data imply the coexistence of two ferromagnetic phases. This peculiar behavior of magnetization curves is quite similar to that of (n-$C_4H_9)_4N[Fe^{II}Fe^{III}(dto)_3]$ in which the LTP and HTP coexist even in the temperature region below the charge transfer phase transition; T_C(LTP) = 7 K and T_C(HTP) = 13 K.[25] In analogy with (n-$C_4H_9)_4N[Fe^{II}Fe^{III}(dto)_3]$, the LTP and HTP individually undergo the ferromagnetic phase transitions in **1** with T_C(LTP) = 5 K and T_C(HTP) = 22 K, respectively. The field dependence of the magnetization at 2 K exhibits the hysteresis loop characteristic of ferromagnetic materials with a coercive field of 1400 Oe. The magnetization at $H = 50000$ Oe yields about 1.90 μ_B. Compound **2** also shows the ferromagnetic transition at 12 K. In this case, the $\chi_M T$ curve exhibits no anomaly, which indicates that the spin configuration of Fe^{II} ($S = 2$) and Fe^{III} ($S = {}^1/_2$) corresponding to the HTP for (n-$C_3H_7)_4N[Fe^{II}Fe^{III}(dto)_3]$ is stable even at 2 K just as (n-$C_5H_{11})_4N[Fe^{II}Fe^{III}(dto)_3]$ and (n-$C_6H_{13})_4N[Fe^{II}Fe^{III}(dto)_3]$. Compounds **3** and **4** are paramagnetic between 2 and 300 K.

Any photoinduced change in the magnetic properties of **2**−**4** was not observed. However, the ferromagnetism of **1** shows a noteworthy response upon UV irradiation. Graphs b and c of Figure 5 show the FCM, RM, and ZFCM curves of **1** after UV irradiation of 350 nm at room temperature. The magnetization

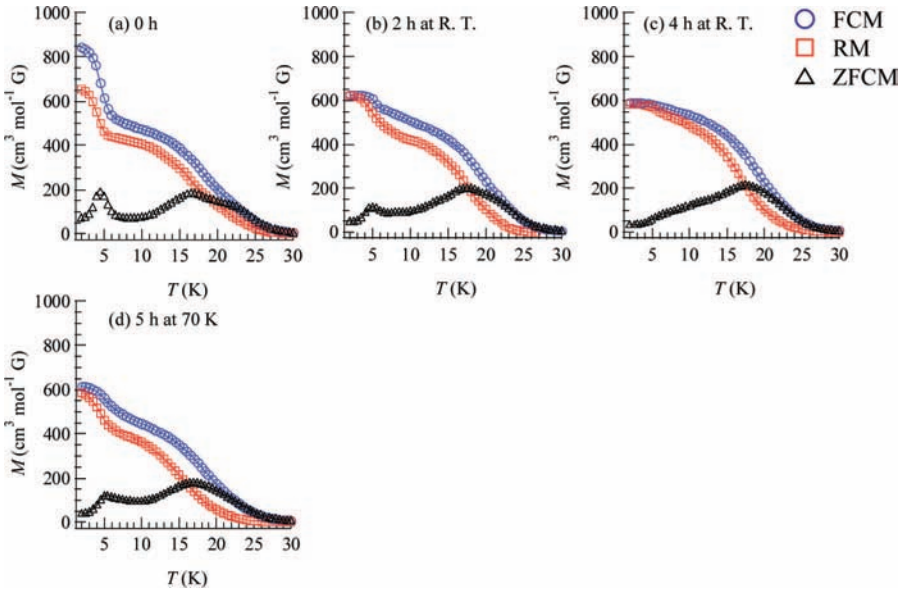

Figure 5. Temperature dependence of FCM, RM, and ZFCM of **1** before (a) and after UV irradiation (350 nm, 40 mW/cm^2) at 300 K (b and c) and 70 K (d). Applied magnetic field was 30 Oe.

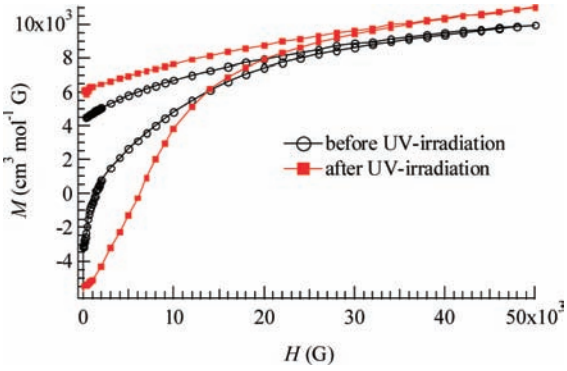

Figure 6. Field dependence of the magnetization of **1** at 2 K before and after UV irradiation (350 nm, 40 mW/cm^2) at room temperature.

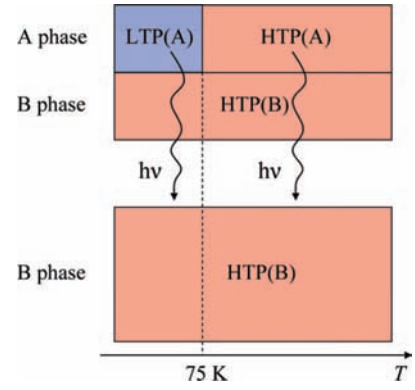

Figure 7. Reaction scheme of **1** before and after UV irradiation.

value below 7 K starts to decrease upon the UV irradiation. The steps in the FCM and RM at 7 K are lowered, and the peak around 5 K in ZFCM disappears, indicating the disappearance of the LTP. On the other hand, the magnetization values between 7 and 30 K are slightly increased after the UV irradiation. Moreover, the thermal hysteresis loop in $\chi_M T$ vs T plot gradually vanishes with the UV irradiation, which is shown in Figure 4d. This photoinduced effect can be explained by the suppression of the charge transfer phase transition. The photoisomerization of SP-Me$^+$ in **1** leads to the expansion of its own volume, which gives a significant stress to the framework of $[Fe^{II}Fe^{III}(dto)_3]^-_\infty$ layers and expands the unit cell volume. Taking into account that the charge transfer phase transition in the $(n\text{-}C_nH_{2n+1})_4N[Fe^{II}Fe^{III}(dto)_3]$ series tends to be inhibited by the expansion of their $(n\text{-}C_nH_{2n+1})_4N^+$ cation size, it can be concluded that the HTP in **1** becomes more stable than the LTP between 2 and 300 K through the medium of the photoisomerization of SP-Me$^+$. In order to elucidate the mechanism of the photoinduced effect on the magnetic properties of **1**, we carried out the control experiment for the magnetism of $(n\text{-}C_4H_9)_4N[Fe^{II}Fe^{III}(dto)_3]$ whose intercalated cation has no photochromic property. After 4 h of UV irradiation (350 nm) at room temperature, the magnetization of $(n\text{-}C_4H_9)_4N[Fe^{II}Fe^{III}(dto)_3]$ shows no change. This result gives a strong evidence that the disappearance of the LTP in **1** after the UV irradiation is caused by the photoisomerization of SP-Me$^+$.

Figure 6 also shows the field dependence of the magnetization at 2 K after 4 h of the UV irradiation at room temperature. The coercive force at 2 K is enhanced from 1400 to 6000 Oe after the UV irradiation. In connection with this, the coercive forces of $(n\text{-}C_nH_{2n+1})_4N[Fe^{II}Fe^{III}(dto)_3]$ at 2 K are 310, 3160, 6600, and 6800 Oe for $n = 3$, 4, 5, and 6, respectively,[26] suggesting the HTP has higher coercive force than the LTP. This result supports the photoinduced HTP giving rise to long-range magnetic ordering.

Before UV irradiation, the charge transfer phase transition occurs around 75 K, while the LTP and HTP coexist below the temperature. There seems to be two phases in **1** from the analysis of the temperature dependence of the magnetic susceptibility. Here we name these phases A and B each. The A phase undergoes the charge transfer phase transition, and the HTP(A) perfectly converts into the LTP(A) with decreasing temperature. On the other hand, the B phase does not undergo the charge transfer phase transition, and the HTP(B) is more stable than the LTP(B) in the whole temperature range. The reaction scheme of **1** is illustrated in Figure 7. Suppose that the UV irradiation induces the transformation from the A to the B phase, the LTP(A) can be forced to convert into the HTP(B) by UV

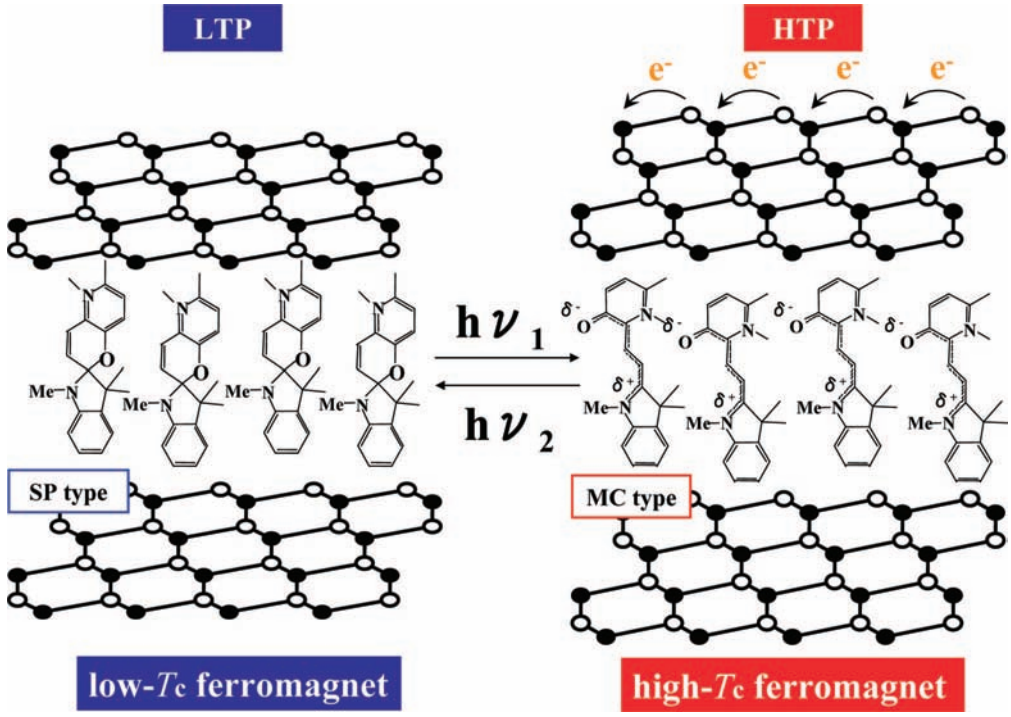

Figure 8. Schematic representation of the concerted phenomenon coupled with the charge transfer phase transition in $[Fe^{II}Fe^{III}(dto)_3]^-_\infty$ and the photoisomerization of spiropyran in (SP-Me)$[Fe^{II}Fe^{III}(dto)_3]$. White circles and black circles are Fe^{II} and Fe^{III}, respectively.

irradiation below 90 K, i.e., the photoisomerization-induced charge transfer phase transition shown in Figure 8 is realized. Here, 90 K is the upper limit of the thermally induced charge transfer phase transition in **1**. In order to confirm the concerted phenomenon coupled with the charge transfer phase transition in $[Fe^{II}Fe^{III}(dto)_3]^-_\infty$ and the photoisomerization of SP-Me^+ in **1**, we performed a low-temperature irradiation experiment which corresponds to the arrow of the left side in Figure 7.[43] The FCM, RM, and ZFCM curves of **1** after the UV irradiation at 70 K are shown in Figure 5d, and the $\chi_M T$ vs T plot of **1** after the UV irradiation is shown in Figure 4c. In fact, the photoinduced change in the magnetic property displays the same tendency as in the case of UV irradiation at 300 K. It should be noted that the destabilization of LTP and the stabilization of HTP under the UV irradiation below 90 K induces the charge transfer phase transition in the $[Fe^{II}Fe^{III}(dto)_3]^-_\infty$ layers. This result proves that the photoisomerization-induced charge transfer phase transition is realized in the system.

The photoisomerization-induced charge transfer phase transition is phenomenologically explained as follows. The free energies of the current system are described as $G_{X,i} = H_{X,i} - S_iT$ (X = A, B phase, i = HTP, LTP). Figure 9 shows the schematic representation of the free energy diagrams of the representative $[Fe^{II}Fe^{III}(dto)_3]$ complexes. In the diagrams, the free energy of the LTP is set to zero in the whole temperature range, and the inclination of $G_{X,HT}$ is equal to $S_{HT} - S_{LT}$. When the orbital degeneracy of the ground state is released due to low symmetrical ligand field, the orbital contribution to the entropy becomes small or negligible, and the spin entropy ($S_{HT} = R \ln 10$, $S_{LT} = R \ln 6$) gives a major contribution to the temperature dependence of the free energy. In connection with this, the following should be mentioned. When the charge transfer phase transition occurs in the heating process, the FeO_6 site expands due to the change from Fe^{III}(HS) to Fe^{II}(HS) while the FeS_6 site shrinks due to the change from Fe^{II}(LS) to Fe^{III}(LS). In this case, the FeO_6 site contributes positively, whereas the FeS_6 site contributes negatively for the vibrational entropy. Consequently, a net contribution to the vibrational entropy is almost canceled. Indeed, the X-ray structural analysis has shown that the space group is unchanged between the HTP and LTP in $(n\text{-}C_3H_7)_4N[Fe^{II}Fe^{III}(dto)_3]$ and moreover, only about 1% change of the unit cell volume is observed at the charge transfer phase transition, which is much smaller than that in normal spin-crossover transition.[25] For example, the unit cell volume changes by about 5% at the low-spin−high-spin transition temperature in $[Fe^{II}(phen)_2(NCS)_2]$ (phen = 1,10-phenanthroline), leading to the large entropy change of 35 J K^{-1} mol^{-1} originating from lattice vibration (73% of the total change).[44] The enthalpy term, on the contrary, decides whether the thermal phase transition occurs; i.e., if $H_{X,HT}$ is lower than $H_{X,LT}$ at the lowest temperature, the crossover of the free energies never happens in the whole range of measuring temperatures. The enthalpy term, however, is considerably affected by pressure, whether external pressure or internal one (so-called chemical pressure effect), in the case of soft materials. In the case of $(n\text{-}C_3H_7)_4N[Fe^{II}Fe^{III}(dto)_3]$, the free energy of LTP should be lower than that of HTP. Therefore, the crossover of the free energies of LTP and HTP takes place at finite temperature, which induces the charge transfer phase transition and denotes its critical temperature, T_{CT}, as the crossover temperature between the free

(43) The sample (1 mg) applied thinly to a copper plate was sandwiched by a quartz glass plate and cooled with a CRYOMINI (Oxford) to 70 K. At this temperature, the sample was irradiated (350 nm, 40 mW/cm^2) for 5 h. After the UV irradiation was stopped, the sample was warmed to room temperature. Then the sample was taken out from the cryostat and the magnetization measurement was performed. Judging from the UV−vis absorption measurement, the photoisomerization-induced HTP is stable enough while the magnetization measurement.

(44) (a) Sorai, M.; Seki, S. *J. Phys. Chem. Solids* **1974**, *35*, 555. (b) Gallois, B.; Real, J.; Hauw, C.; Zarembowitch, J. *Inorg. Chem.* **1990**, *29*, 1152.

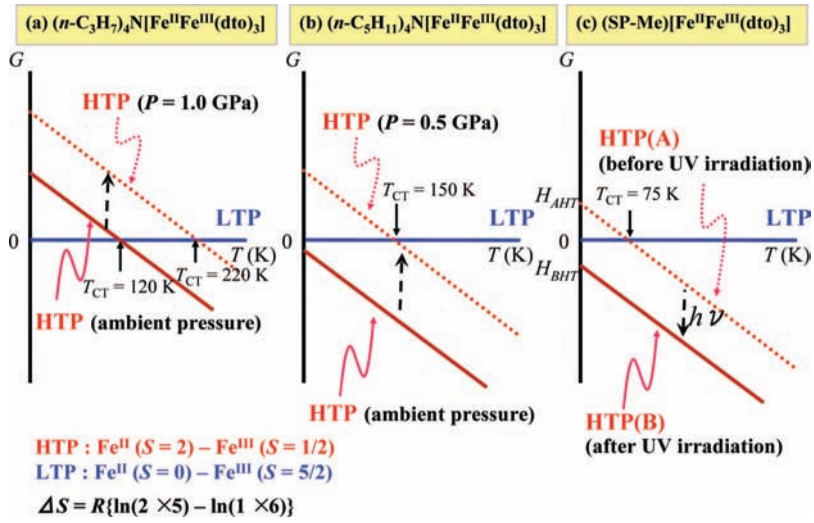

Figure 9. Schematic phase diagram of $[Fe^{II}Fe^{III}(dto)_3]$ complexes. The vertical axes are the free energy relative to the LTP. The inclination of the HTP takes into account only spin entropy. The intercepts correspond to the difference of the enthalpy between the HTP and the LTP at 0 K.

energy of LTP and HTP. In this phase diagram, an external pressure stabilizes and destabilizes the LTP and HTP, respectively, which increases the crossover temperature. In fact, T_{CT} for $(n\text{-}C_3H_7)_4N[Fe^{II}Fe^{III}(dto)_3]$ remarkably increases by 100 K with increasing hydrostatic pressure up to 1 GPa.[45] In the case of $(n\text{-}C_5H_{11})_4N[Fe^{II}Fe^{III}(dto)_3]$, on the other hand, the free energy of HTP should be lower than that of LTP as shown Figure 9b. Therefore, the charge transfer phase transition does not take place in the whole temperature region. In this case, the free energy of HTP increases with increasing external pressure, and eventually the crossover of the free energies between LTP and HTP appears which induces the sudden appearance of the charge transfer phase transition. Actually, the charge transfer phase transition suddenly appears around 150 K in $(n\text{-}C_5H_{11})_4N[Fe^{II}Fe^{III}(dto)_3]$ when the pressure of 0.5 GPa is applied.[46] This external pressure effect presumably stabilizes the LTP relative to the HTP, which is the opposite tendency to the negative chemical pressure effect by substituting the larger countercation. The photoisomerization of SP-Me^+ in **1** changes the enthalpy from H_A to H_B, which leads the HTP to an enough stabilization to inhibit the charge transfer phase transition ($G_{A,HT}$ to $G_{B,HT}$) or convert the LTP into the HTP ($G_{A,LT}$ to $G_{B,HT}$), which is shown in Figure 9c.

In summary, we synthesized a photosensitive organic−inorganic hybrid system, $(SP\text{-}Me)[Fe^{II}Fe^{III}(dto)_3]$, in order to control the magnetic properties and the electronic state by means of photoisomerization of SP-Me^+. This compound undergoes the charge transfer phase transition with large thermal hysteresis around 75 K, and two ferromagnetic phases coexist, with T_C = 5 K and T_C = 22 K, corresponding respectively to the LTP with $Fe^{II}(S = 0)$−$Fe^{III}(S = {}^5/_2)$ and the HTP with $Fe^{II}(S = 2)$−$Fe^{III}(S = {}^1/_2)$. In this system, the photoisomerization of the intercalated spiropyran from the CF to the OF by UV irradiation and from the OF to the CF by visible-light irradiation reversibly takes place at 70 K as well as at room temperature. The photoisomerization by UV irradiation at room temperature suppresses the charge transfer phase transition, leading to the change of the Curie temperature from 5 to 22 K and the coercive force from 1400 to 6000 Oe. Moreover, The photoisomerization by UV irradiation at 70 K induces the concerted phenomenon coupled with the charge transfer phase transition in $[Fe^{II}Fe^{II-I}(dto)_3]^-_\infty$ and the photoisomerization of spiropyran.

This new type of photomagnetism coupled with spin, charge, and photon is triggered by a chemical pressure effect generated from the photoisomerization of spiropyran from the close form to the open one in the complex. This situation seems to have significant similarity with the first events in the perception of light in rhodopsin in which photoisomerization of 11-*cis*-retinal into all-*trans*-retinal induces a conformational change in opsin and activates the associated G protein and triggers a second messenger cascade.

Acknowledgment. We thank Prof. H. Kobayashi and Dr. K. Takahashi for valuable discussions on the structural analysis and Dr. Y. Ono for valuable assistance with the Mössbauer experiments. This work was supported by a Grant-in-Aid for Scientific Research, a Grant-in-Aid of the 21st century COE (Center of Excellence) Program, and a Grant-in-Aid for Scientific Research on Priority Areas from the Ministry of Education, Culture, Sports, Science and Technology, Japan. M.I. and M.O. were supported by Research Fellowships of the Japan Society for the Promotion of Science for Young Scientists.

JA806879A

(45) Kobayashi, Y.; Itoi, M.; Kojima, N.; Asai, K. *J. Phys. Soc. Jpn.* **2002**, *71*, 3016.
(46) Kobayashi, Y.; Itoi, M.; Kojima, N.; Asai, K. *J. Mag. Mag. Mater.* **2004**, *272*−*276*, 1091.